Transitions between liquid crystalline phases investigated by dielectric and infra-red spectroscopies

Aleksandra Deptuch^{1,*}, Natalia Osiecka-Drewniak¹, Anna Paliga², Natalia Górska³, Anna Drzewicz¹, Katarzyna Chat¹, Mirosława D. Ossowska-Chruściel⁴, Janusz Chruściel⁴

Abstract

The liquid crystalline 11OS5 compound, forming the nematic phase and a few smectic phases, is investigated by broadband dielectric spectroscopy and infra-red spectroscopy. The dielectric relaxation times, ionic conductivity, and positions of infra-red absorption bands corresponding to selected intra-molecular vibrations are determined as a function of temperature in the range from isotropic liquid to a crystal phase. The correlation coefficient matrix and k-means cluster analysis of infra-red spectra are tested for detection of phase transitions. The density-functional theory calculations are carried out for interpretation of experimental infra-red spectra. The performance of various basis sets and exchange-correlation functionals is compared, including both agreement of scaled calculated band positions with experimental values and computational time. The intermolecular interactions in the crystal phase are inferred from the experimental IR spectra and density-functional theory calculations for dimers in head-to-head and head-to-tail configurations. The experimental temperature dependence of the C=O stretching band suggests that the head-to-tail configuration in a crystal phase is more likely. A significant slowing down of the flip-flop relaxation process is observed at the transition between the smectic C and hexagonal smectic X phases.

1. Introduction

The broadband dielectric spectroscopy (BDS) gives insight into the relaxation processes of dipoles in a weak, alternating electric field [1]. In liquid crystals, it involves molecular processes – rotations of molecules around their short and long axes and, in some cases, also collective processes – fluctuations of order parameters [2]. The BDS method is applied for identification of liquid crystalline phases [3-5], determination of phase transition temperatures [5-7], as well as investigation of the glass transition [5,8] and crystallization kinetics [8,9]. The complementary infra-red (IR) spectroscopy reveals the intra-molecular vibrations which change a molecule's dipole moment [10]. This method is applied for investigation of the sample's purity [11,12], molecular conformation [13,14], and

¹ Institute of Nuclear Physics Polish Academy of Sciences, Radzikowskiego 152, PL-31342 Kraków, Poland

² Faculty of Physics, Astronomy and Applied Computer Science, Jagiellonian University, Łojasiewicza 11, PL-30348 Kraków, Poland

³ Faculty of Chemistry, Jagiellonian University, Gronostajowa 2, PL-30387 Kraków, Poland

⁴ Faculty of Science, University of Siedlee, 3 Maja 54, PL-08110 Siedlee, Poland

^{*} corresponding author, aleksandra.deptuch@ifj.edu.pl

intermolecular interactions [14,15]. Some IR absorption bands are sensitive to phase transitions, especially these related to significant changes in structure, like melting of a crystal [14,15].

The purpose of this study is analysis of the dielectric and IR spectra of 4-pentylphenyl-4'-undecyloxythiobenzoate, denoted as 11OS5 (Figure 1), focused on transitions between the mesomorphic and crystal phases of this compound. 11OS5 forms several thermotropic liquid crystalline phases between isotropic liquid (Iso) and crystal (Cr) [16]:

- Nematic (N) with a long-range orientational order of long molecular axes [17].
- Smectic A (SmA) with a quasi-long-range lamellar order and zero average tilt of molecules within smectic layers [17].
- Smectic C (SmC) with quasi-long-range lamellar order and non-zero average tilt of molecules within smectic layers [17]. The tilt angle in the SmC phase of 11OS5, estimated from the X-ray diffraction patterns, reaches only 11° [16].
- Smectic X (SmX), a crystal-like tilted smectic phase with a long-range positional order described by a monoclinic unit cell and a hexagonal intra-layer order. It is either the SmG phase with the unit cell parameters $b < \alpha < c$, $\alpha = \gamma = 90^{\circ}$, $\beta \neq 90^{\circ}$ or the SmJ phase with $\alpha < b < c$, $\alpha = \gamma = 90^{\circ}$, $\beta \neq 90^{\circ}$ [17]. The X-ray diffraction data from [16] do not enable distinction between these phases, which differ only by the direction of a molecular tilt in respect to a hexagonal ordering within layers [17]. The tilt angle of molecules in the SmX phase of 11OS5 is equal to ca. 15° [16].
- Smectic Y' and Y, crystal-like smectic phases, with a long-range positional order described by the monoclinic unit cells and probably a herring-bone intra-layer order [17]. The X-ray diffraction patterns of these phases were not obtained due to quick crystallization [16].

The phase sequence of 11OS5 during cooling at 5 K/min is Iso (357.4 K) N (355.9 K) SmA $\{338\}$ SmC (326.0 K) SmX (298.5 K) SmY' (296.0 K) SmY (294.7 K) Cr, where temperatures in () were determined by differential scanning calorimetry and temperature in $\{\}$ was determined by polarizing optical microscopy, because the SmA \rightarrow SmC transition was not visible in the calorimetric results [16]. The SmX, SmY', SmY phases are metastable and they are observed only after supercooling below the melting temperature of a crystal, which is 334 K [16]. However, 11OS5 remains in the metastable SmX phase long enough to enable conducting measurements in isothermal conditions before crystallization occurs [16].

In the first part, the relaxation times, dielectric strength, and ionic conductivity are obtained as a function of temperature from the BDS spectra of 11OS5 collected on cooling. In the second part, the experimental IR spectrum of 11OS5 in a crystal phase at the room temperature is analyzed based on theoretical spectra calculated at various levels of theory. The experimental IR absorption bands are assigned to particular intra-molecular vibrations and performances of different levels of theory (scaling coefficients, root-mean square error, computational times) are compared. In the third part,

the IR spectra of 11OS5 collected on cooling are analyzed using the matrix of correlation coefficients [18] and k-means cluster method [19-21]. Positions of selected IR absorption bands are investigated as a function of temperature. The main aim is an attempt to detect subtle changes in the BDS and IR spectra related to the SmA \rightarrow SmC transition as well as to investigate more significant changes related to the SmC \rightarrow SmX transition. The comparison of BDS and IR data may enable correlation of dielectric relaxation with intra-molecular vibrations for better understanding of molecular rearrangements during phase transitions between mesophases and a crystalline state.

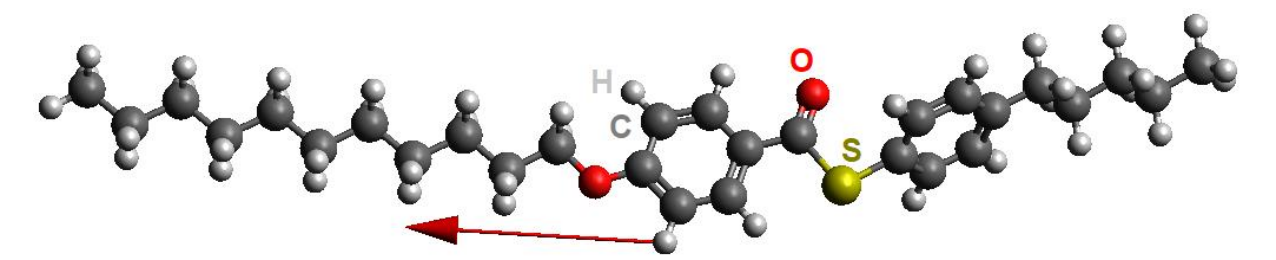


Figure 1. The 11OS5 molecular model and its dipole moment (2.4 D) optimized by the DFT method (def2TZVPP basis set, B3LYP-D3(BJ) functional).

2. Experimental and computational details

The synthesis of 4-pentylphenyl-4'-undecyloxythiobenzoate, abbreviated as 11OS5, is described elsewhere [22]. The IR results presented in this work confirm the molecular structure.

The BDS measurements were performed using the Novocontrol Technologies spectrometer for a sample with a thickness of 75 μ m, placed between two golden electrodes with the polytetrafluoroethylene spacer. The dielectric spectra were collected on cooling from 373 K to 273 K, in the frequency range of 0.1-10⁷ Hz. The data were analyzed by fitting the complex model of the dielectric permittivity vs. frequency in OriginPro.

The Fourier-transform IR measurements were performed using the Bruker VERTEX 70v FT-IR spectrometer equipped with Advanced Research System DE-202A cryostat and ARS-2HW compressor. The IR spectra were collected by the attenuated total reflection method for a pure sample at the room temperature in the wavenumber range of 370-4000 cm⁻¹ and by the transmission method for a sample mixed with KBr on cooling from 373 K to 273 K in the wavenumber range of 450-4000 cm⁻¹, both with a resolution of 2 cm⁻¹.

The correlation coefficient matrix of IR spectra collected in different temperatures was calculated using a Python script based on the SciPy and NumPy libraries [23]. The fitting of pseudo-Voigt peak functions with a linear background to selected absorption bands and k-means cluster analysis with the Euclidean metrics [19] were carried out in OriginPro. The background subtraction was performed before calculation of the correlation coefficient matrix and k-means cluster analysis.

The assignment of the IR absorption bands was based on the theoretical IR spectra calculated by the DFT method at various levels of theory for an isolated molecule in Gaussian 16, Revision C.01 [24]. The tested basis sets were def2SVP, def2SVPP, def2TZVP, def2TZVPP [25,26], 631+Gd, and 6311+Gdp [27-30]. The applied exchange-correlation functionals were either BLYP-D3(BJ) or B3LYP-D3(BJ) [31-33]. The contributions of vibrational modes were calculated via the potential energy distribution analysis in VEDA [34,35].

3. Results and discussion

3.1. Dielectric spectra vs. temperature

The BDS spectra of 11OS5 (Figure 2) were fitted with the complex function including the Cole-Cole model of relaxation processes, contribution from conductivity in the imaginary part ε'' , and electrode polarization contribution in the real part ε' of dielectric permittivity ε^* [2,36]:

$$\varepsilon^*(f) = \varepsilon'(f) - i\varepsilon''(f) = \varepsilon_{\infty} + \sum_{j} \frac{\Delta \varepsilon_j}{1 + (2\pi i f \tau_j)^{1 - a_j}} - \frac{is_1}{(2\pi f)^{n_1}} + \frac{is_2}{(2\pi f)^{n_2}}.$$
 (1)

The Cole-Cole model describes each relaxation processes by the dielectric strength $\Delta \varepsilon$, relaxation time τ , and parameter a, corresponding to the distribution of the relaxation time (for the Debye model, a=1); ε_{∞} is the dielectric dispersion in the limit of high frequencies; s_1 , n_1 and s_2 , n_2 are fitting parameters of the background at low frequencies, originating from the sample's conductivity and electrode polarization, respectively, or from the tails of low-frequency relaxation processes. The BDS results are summarized in Figure 3. The phase transitions are visible as significant discontinuities in the temperature dependence of the dielectric dispersion registered at ca. 1 kHz. The exception is the SmA \rightarrow SmC transition, which corresponds to a very small step in the $\varepsilon'(1 \text{ kHz}, T)$ plot. The hexagonal SmX, despite it is metastable, is observed in a temperature range wider than 15 K, while the SmY', SmY phases are not detected and the direct SmX \rightarrow Cr transition occurs.

Two relaxation processes are observed in the isotropic liquid, nematic, SmA and SmC phases. The fitting results of Equation (1) are presented only for temperatures below the Iso \rightarrow N transition, because in the isotropic liquid, some of the fitting parameters had too large uncertainties. The low-frequency process, with the average $\Delta \varepsilon = 5.9$, a = 0.11 and activation energy $E_a = 79(2)$ kJ/mol, is interpreted as the Maxwell-Wagner-Sillars process [37]. The high-frequency process, with the average $\Delta \varepsilon = 0.11$, a = 0.01 and activation energy $E_a = 94.2(4)$ kJ/mol, is the molecular s-process, originating from rotations of molecules around their short axes (called also flip-flop motions) [6,38,39]. The presented activation energies were obtained in the SmA and SmC phases. For the N phase, which has a narrow temperature range, only two BDS spectra were collected and the activation energies were not determined. The conductivity contribution in the low-frequency region of ε'' can be fitted with an assumption of ionic conductivity, where $n_1 = 1$ [40]. The conductivity determined as $\sigma = s_1 \varepsilon_0$, where ε_0 is the vacuum permittivity, shows the linear dependence in the activation plot, with $E_a = 97(3)$

kJ/mol. The polarization contribution in the nematic phase is described by $n_2 = 1.5$, in agreement with [40], while in SmA and SmC, this contribution was fixed to zero. The activation energies of the s-process obtained earlier for the SmA and SmC phases in nOS5 homologs with n = 8, 9, 10 are in the 92-110 kJ/mol range [41], comparable to the result for 11OS5.

In the hexagonal SmX phase, the s-process shifts abruptly to lower frequencies. The ratio of τ in the SmX and SmC phases at the SmC \rightarrow SmX transition is equal to 46. The dielectric strength of the s-process decreases to $\Delta\varepsilon=0.07$ and the activation energy increases to 144(1) kJ/mol. The observed changes are caused by arise of the positional order within the smectic layers. The Cole-Cole parameter equals on average a=0.04, thus, the s-process still has an almost ideally Debye character. The conductivity part cannot be correctly described under an assumption of $n_1=1$. The fitted values of n_1 are equal to 0.8-0.9 and only shortly before crystallization, $n_1=0.4$. The activation energy of σ , which is only an effective conductivity if $n_1 \neq 1$, is equal to 99(2) kJ/mol. Thus, the SmC \rightarrow SmX transition leads to decrease in conductivity, but E_a is the same within uncertainties. The polarization contribution also is not anymore described by $n_2=1.5$, as it was in the nematic phase. Instead, n_2 gradually decreases on cooling from 1.1 to 0.6. Deviation from $n_2=1.5$ may be caused by the Maxwell-Wagner relaxation, which is out of the measured frequency range, but the high-frequency tail still affects the collected spectra.

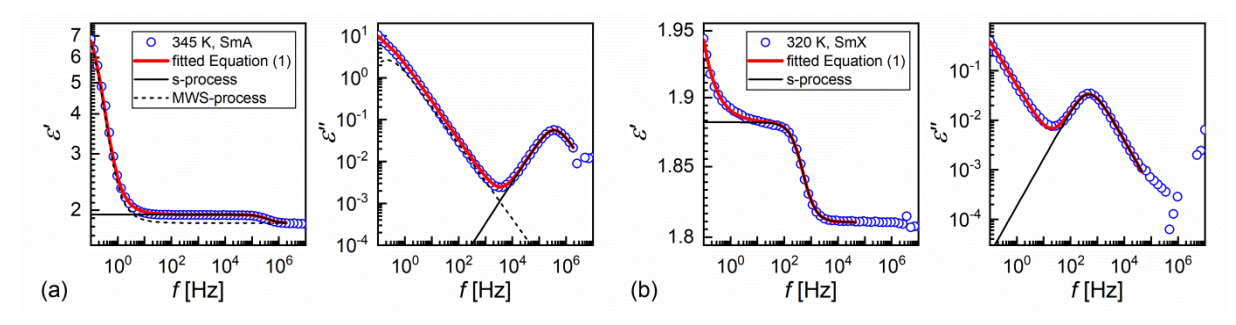


Figure 2. Exemplary BDS spectra of 11OS5 in the SmA (a) and SmX (b) phases with the fitting results of Equation (1).

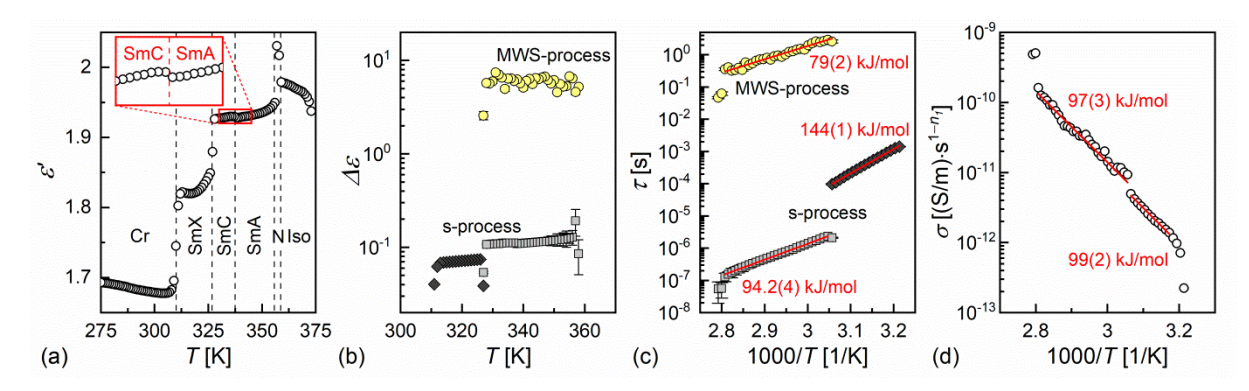


Figure 3. Dielectric dispersion at 1 kHz (a) and dielectric strength of relaxation processes in 11OS5 (b) as a function of temperature; activation plots of the relaxation times (c) and conductivity (d).

3.2. Scaling of calculated infra-red spectra

The assignment of IR absorption bands to intra-molecular vibrations was performed for the IR spectrum collected in the reflection mode at the room temperature for 11OS5 in a crystal phase (Figure 4). The theoretical band positions and intensities were calculated using the triple-zeta basis sets def2TZVPP, def2TZVP; split-valence basis sets def2SVPP, def2SVP; and 631+Gd, 6311+Gdp basis sets with diffuse corrections. The Becke exchange functional and Lee-Yang-Parr correlation functional were applied as BLYP and B3LYP functionals together with the Grimme's 3D dispersion and Becke-Johnson damping (see Section 2 for references). The calculated spectra are shown in Figure 4 below the experimental result. The band assignments as well as the comparison of experimental and calculated band positions are gathered in Tables S1-S8 in the Supplementary Materials (SM).

The scaling coefficient a relates experimental \tilde{v}_{exp} and calculated \tilde{v}_{calc} band positions as follows: $\tilde{v}_{exp} = a\tilde{v}_{calc}$. It is determined as a slope of the linear fit to the $\tilde{v}_{exp}(\tilde{v}_{calc})$ plot, with the intercept fixed to zero (Figure S1 in SM). The fitting can be performed in the full wavenumber range. However, it is advised to determine it separately for the <1000 cm⁻¹, 1000-2000 cm⁻¹, and >2000 cm⁻¹ ranges [42]. The results for 11OS5 (Table 1) show that the scaling coefficients at the same level of theory are larger and closer to 1 for the bands located below 2000 cm⁻¹ than for these at higher wavenumbers. The scaling coefficients obtained for <1000 cm⁻¹ and 1000-2000 cm⁻¹ have close values, in some cases even equal within the uncertainty. In all cases where the B3LYP-D3(BJ) functional was applied, a < 1, which means that calculated band positions are overestimated. The BLYP-D3(BJ) functional leads to underestimation of band positions only below 2000 cm⁻¹, a > 1, while the linear fit performed at higher wavenumbers and in the whole range gives a < 1.

The root-mean square error between the experimental and scaled calculated band positions was obtained as $RMSE = \sqrt{\frac{1}{n}\sum_{i=1}^{n}(\tilde{v}_{expi} - a\tilde{v}_{calci})^2}$, where n is the number of bands. Different values of a were used in the <1000 cm⁻¹, 1000-2000 cm⁻¹, and >2000 cm⁻¹ ranges, according to Table 1. The overall scaling factor (column 'all' in Table 1) was not used in calculation of RMSE. The smallest RMSE values are 11.6 cm⁻¹ for def2TZVPP/B3LYP-D3(BJ) and 11.9 cm⁻¹ for def2TZVP/B3LYP-D3(BJ). The corresponding computational time is 156.9 h and 85.8 h, respectively. Thus, the longest def2TZVPP/B3LYP-D3(BJ) calculations do not give a significant improvement in RMSE compared to twice as short def2TZVP/B3LYP-D3(BJ) calculations. The third smallest RMSE, 12.5 cm⁻¹, is obtained for 631+Gd/B3LYP-D3(BJ), with a relatively short computational time, 17.6 h. Interestingly, much longer 6311+Gd/B3LYP-D3(BJ) calculations lasting 40.7 h give slightly worse RMSE equal to 13.1 cm⁻¹. One of the shortest are def2SVP/BLYP-D3(BJ) calculations, lasting 4.7 h, and the corresponding RMSE is 13.6 cm⁻¹. The BLYP-D3(BJ) functional shows a worse performance when used with the 631+Gd basis set, because the computational time is longer (8.8 h) and RMSE is larger (15.1 cm⁻¹) than for the def2SVP basis set. The largest RMSE values are 17.1 cm⁻¹ for

def2SVPP/B3LYP-D3(BJ) and $17.8~cm^{-1}~def2SVP/B3LYP-D3(BJ)$, with the computational times 4.7 h and 6.6 h, respectively.

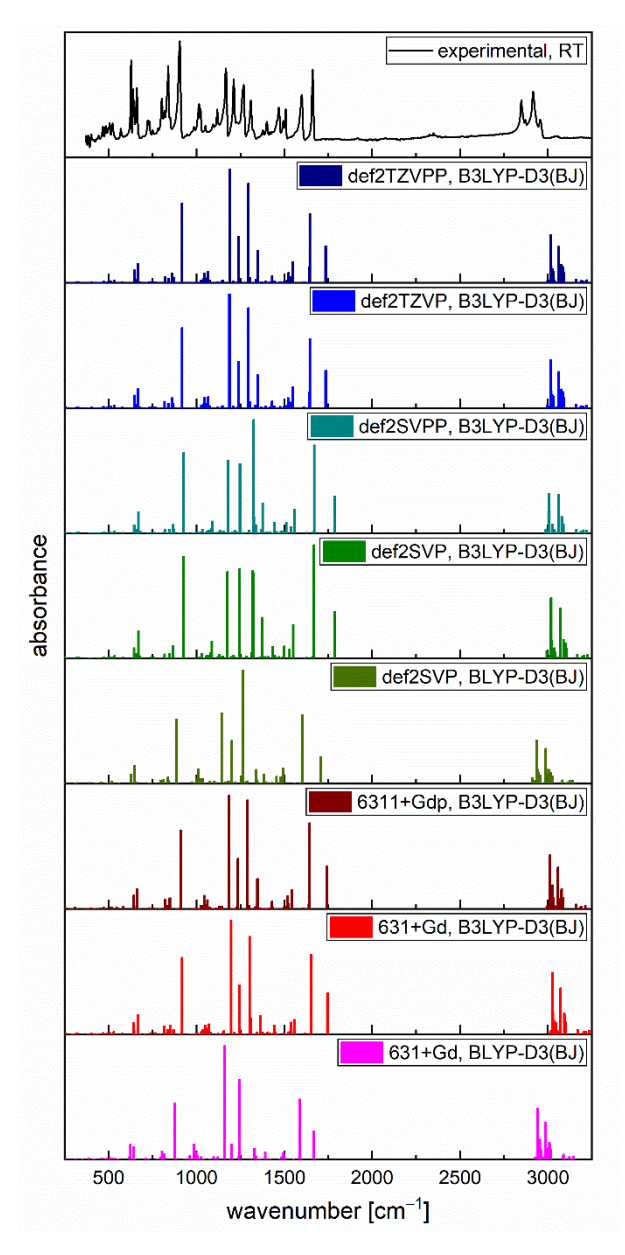


Figure 4. Experimental IR spectrum of 11OS5 in a crystal phase at the room temperature compared to unscaled spectra calculated by the DFT method at different levels of theory.

Table 1. Scaling factors between experimental and calculated IR band positions determined for 11OS5. The first column refers to the detailed IR band assignments shown in SM. The root mean square error (*RMSE*) was calculated for experimental and scaled calculated band positions using the scaling factors obtained separately for the <1000 cm⁻¹, 1000-2000 cm⁻¹, and >2000 cm⁻¹ ranges. The cpu times were taken from the Gaussian output files.

table basis set		functional	scaling factor			RMSE	cpu time [h]	
table basi	basis set	basis set functional	$<1000~{\rm cm}^{-1}$	$1000\text{-}2000~\text{cm}^{-1}$	$>2000~{\rm cm}^{-1}$	all	$[cm^{-1}]$	cpu time [ii]
S1	def2TZVPP	B3LYP-D3(BJ)	0.974(4)	0.974(2)	0.952(2)	0.961(2)	11.6	156.9
S2	def2TZVP	B3LYP-D3(BJ)	0.975(4)	0.974(2)	0.952(2)	0.962(2)	11.9	85.8
S 3	def2SVPP	B3LYP-D3(BJ)	0.966(5)	0.960(4)	0.952(2)	0.952(2)	17.1	4.7
S4	def2SVP	B3LYP-D3(BJ)	0.969(5)	0.965(4)	0.950(2)	0.957(2)	17.8	6.6
S5	def2SVP	BLYP-D3(BJ)	1.005(3)	1.003(3)	0.975(2)	0.988(3)	13.6	4.7
S 6	6311+Gdp	B3LYP-D3(BJ)	0.978(4)	0.975(3)	0.953(2)	0.963(2)	13.1	40.7
S 7	631+Gd	B3LYP-D3(BJ)	0.977(4)	0.966(3)	0.947(2)	0.957(2)	12.5	17.6
S8	631+Gd	BLYP-D3(BJ)	1.014(4)	1.004(4)	0.974(2)	0.988(3)	15.1	8.8

3.3 Infra-red spectra vs. temperature

The IR spectra of 11OS5 were collected on cooling from 373 K to 273 K in the transmission mode (Figure 5). The spectra in the isotropic liquid, nematic, and smectic phases are very similar and only crystallization shows as sharpening of absorption bands. Three methods are applied to search for the subtle differences in IR spectra in higher temperatures: (1) calculation of the correlation coefficients matrix, (2) k-means cluster analysis, and (3) determination of the selected absorption bands' positions as a function of temperature.

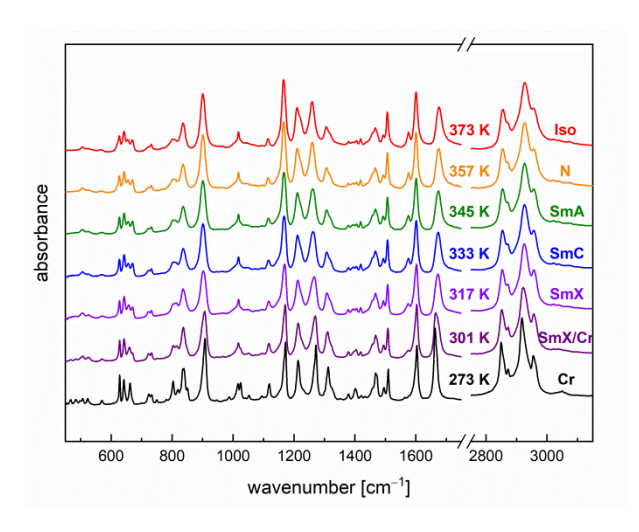


Figure 5. Representative experimental IR spectra of 11OS5 collected on cooling.

The correlation coefficient of two datasets is defined as [18]:

$$r = \frac{\sum_{i=1}^{n} (x_i - \bar{x})(y_i - \bar{y})}{(n-1)s_x s_y},$$
(2)

where x_i , y_i are values obtained at different temperatures, \bar{x} , \bar{y} are mean values, s_x , s_y are standard deviations, n is a number of (x_i, y_i) pairs. The matrix of the correlation coefficients of the IR spectra of 11OS5 is presented in Figure 6a. The data can be divided into four clusters: {373, 369, 365, 357 K}

– Iso and N; {353, 349, 345, 341, 337, 333, 329 K} – SmA and SmC; {325, 321, 317, 313, 309, 305 K} – SmX; 301 K – crystallization; {297, 293, 289, 285, 281, 277, 273 K} – crystal. The correlation coefficients for some temperatures (e.g. 317 K) enable distinction of the N phase at 357 K (Figure 6b). The SmA → SmC transition does not show in the correlation coefficient matrix.

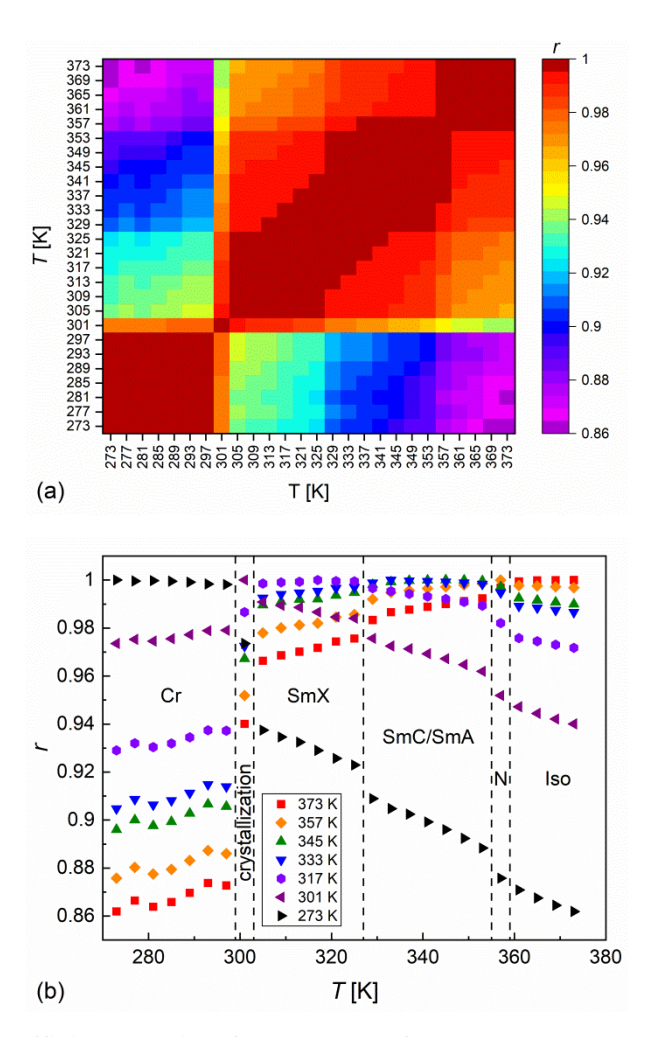


Figure 6. Correlation coefficient matrix of IR spectra of 11OS5 (a) and correlation coefficients for selected spectra as a function of temperature (b).

The k-means cluster analysis is based on an algorithm which separates data into clusters with maximal similarity of data within each cluster and maximal difference of data between clusters [19-21]. The optimal number of clusters indicated by the "elbow method" [20] is four (Figure S2 in SM). The true number of clusters in the dataset is unknown. The elbow method is a heuristic technique used to estimate the optimal number of clusters by identifying the point where increasing the number of clusters no longer significantly reduces the within-cluster variance. The 4-cluster analysis performed for IR spectra in the whole range divides data as follows: {373, 369, 365, 357 K} – Iso and N; {353, 349, 345, 341, 337, 333, 329, 325, 321 K} – SmA, SmC, and SmX; {317, 313, 309, 305, 301 K} – SmX and crystallization; {297, 293, 289, 285, 281, 277, 273 K} – crystal. Thus, the 4-cluster

analysis for full spectra is sensitive to the $N \to SmA$ and $SmX \to Cr$ transitions, but does not separate correctly the temperature ranges of SmC and SmX. The Iso and N phase are not distinguished, same as SmA and SmC. In the next step, the 4-cluster analysis was performed separately for selected spectral ranges to find out which intra-molecular vibrations are sensitive to particular phase transitions:

- 450-590 cm⁻¹ out-of-plane deformations of both aromatic rings, in-plane deformations of the aromatic ring next to the alkoxy chain, scissoring of C-S-C, scissoring of C-C-C and C-O-C in the alkoxy chain,
- 590-685 cm⁻¹ out-of-plane deformations of the aromatic ring next to the alkoxy chain, inplane deformations of both aromatic rings, out-of-plane deformations of the COS group,
- 685-760 cm⁻¹ out-of-plane deformations of the aromatic ring next to the alkyl chain, rocking of CH₂ groups in both terminal chains,
- 760-860 cm⁻¹ out-of-plane deformations of both aromatic rings, in-plane deformations of the aromatic ring next to the alkoxy chain, rocking of CH₂ groups in the alkoxy chain, twisting of CH₂ groups in the alkyl chain
- 860-930 cm⁻¹ in-plane deformations of the aromatic ring next to the alkoxy chain, C-S stretching in the COS group,
- 930-1065 cm⁻¹ stretching of C-C and C-O bonds in the alkoxy chain,
- 1065-1190 cm⁻¹ in-plane deformations of both aromatic rings, stretching of C-C bonds in the alkoxy chain,
- 1190-1290 cm⁻¹ in-plane deformations of the aromatic ring next to the alkoxy chain, wagging of CH₂ groups in the alkyl chain,
- 1290-1345 cm⁻¹ in-plane deformations of both aromatic rings, wagging of CH₂ groups in the alkyl chain,
- 1345-1426 cm⁻¹ in-plane deformations of the aromatic ring next to the alkyl chain, wagging of CH₂ groups in both terminal chains,
- 1426-1482 cm⁻¹ scissoring of CH₂ groups in both terminal chains,
- 1482-1550 cm⁻¹ in-plane deformations of both aromatic rings, scissoring of CH₂ groups in the alkoxy chain,
- 1550-1625 cm⁻¹ in-plane deformations of the aromatic ring next to the alkoxy chain,
- $1625-1750 \text{ cm}^{-1}$ stretching of C=O bond,
- $2700-3150 \text{ cm}^{-1}$ stretching of C-H bonds.

The band assignment is based on the def2TZVPP/B3LYP-D3(BJ) calculations in Gaussian [24] and potential energy distribution analysis in VEDA [34,35] (Table S1). The results of 4-cluster analysis identical with these of full IR spectra are obtained for two spectral ranges (Figure 7): 590-685 cm⁻¹ (deformations of aromatic rings and out-of-plane deformation of COS) and 1426-1482 cm⁻¹ (scissoring of CH₂ groups). The absorption bands sensitive to the Iso \rightarrow N transition in the 4-cluster

analysis are these in the 2700-3150 cm⁻¹ range (stretching of C-H bonds). The N \rightarrow SmA transition is indicated by bands at 590-685 cm⁻¹, 760-860 cm⁻¹, 1065-1190 cm⁻¹, and 1290-1750 cm⁻¹ (deformations of aromatic rings, out-of-plane deformation of the COS group, rocking, wagging, twisting, and scissoring of CH₂ groups, stretching of C-C and C=O bonds). The SmA and SmC phases are separated correctly for bands at 685-760 cm⁻¹ (out-of-plane deformations of the aromatic ring next to the alkyl chain, rocking of CH₂ groups). The SmC \rightarrow SmX transition is indicated by bands at 860-930 cm⁻¹, 1065-1290 cm⁻¹, and 1482-1625 cm⁻¹ (deformations of aromatic rings, stretching of C-S in the COS group, stretching of C-C bonds, wagging and scissoring of CH₂ groups). The crystallization is detected by all bands. However, the analysis for bands at 450-590 cm⁻¹, 685-760 cm⁻¹, and 930-1065 cm⁻¹ (deformations of aromatic rings, scissoring of C-S-C, C-C-C, C-O-C, stretching of C-C, C-O bonds, rocking of CH₂ groups) separates the spectrum collected at 273 K from other spectra collected in the 277-297 K range, which may indicate some structural changes within a solid state.

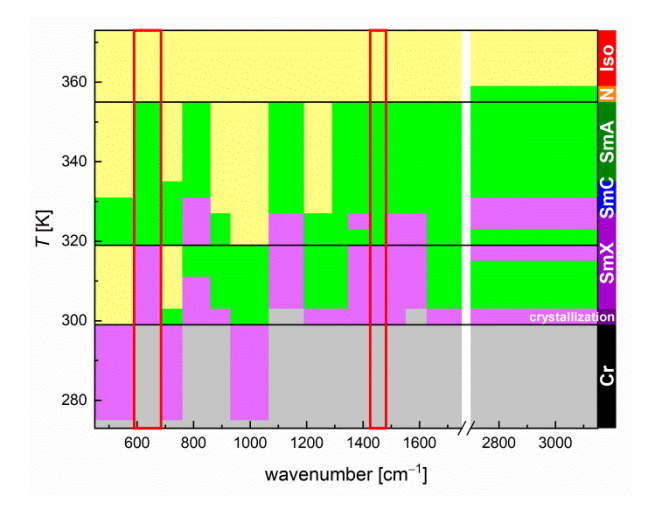


Figure 7. Results of the 4-cluster analysis for selected ranges in the IR spectra of 11OS5. Horizontal lines indicate borders between clusters obtained for full IR spectra. Red frames indicate spectral ranges with identical clusters as obtained for full spectra.

Finally, the temperature behavior of two selected absorption bands is investigated (Figure 8). The first band is the one located at $1663\text{-}1674~\text{cm}^{-1}$, corresponding to the C=O stretching (vC=O). The second band in the one located at $901\text{-}909~\text{cm}^{-1}$, corresponding to the in-plane deformations of the aromatic ring close to the alkoxy chain ($\beta_{asym}Ph_{alkoxy}$) and C-S stretching in the COS group (vCS). Each band is well-separated from neighbor absorption bands. The band related to vC=O shows a redshift (decrease of the band position) at transitions from the less ordered to more ordered phases on cooling, which is explained by formation of weak hydrogen bonds [43,44]. The largest redshift of almost 8 cm⁻¹ occurs between the SmX and crystal phases. The redshift at the SmC \rightarrow SmX transition is very small, less than 1 cm⁻¹, and comparable to the redshift observed at the Iso \rightarrow N \rightarrow SmA transitions. No redshift occurs at the SmA \rightarrow SmC transition. The band related to $\beta_{asym}Ph_{alkoxy}$ and vCS

vibrations shows the opposite behavior, which is a blueshift (increase of the band position) on cooling. The blueshift at the SmX \rightarrow Cr and SmC \rightarrow SmX transitions is 4 cm⁻¹ and 1 cm⁻¹, respectively, while it is negligible at transitions at higher temperatures.

The influence of intermolecular interactions on IR spectra was modelled by DFT calculations for dimers. The head-to-head and head-to-tail dimers of 11OS5 were optimized (Figure 9) and corresponding IR spectra were calculated using the 631+Gd basis set and B3LYP-D3(BJ) functional (Figure 10), which gave reasonably low RMSE and short computational time in calculations for an isolated molecule (Table 1). The theoretical band position at the 631+Gd/B3LYP-D3(BJ) level related to vC=O is 1746 cm⁻¹ for an isolated molecule (Table S7 in SM), 1741, 1756 cm⁻¹ for a headto-head dimer, and 1726, 1740 cm⁻¹ for a head-to-tail dimer. The theoretical band position at the 631+Gd/B3LYP-D3(BJ) level related to $\beta_{asym}Ph_{alkoxy}$ and νCS is 919 cm⁻¹ for an isolated molecule (Table S7 in SM), 912, 922 cm⁻¹ for a head-to-head dimer, and 915, 920 cm⁻¹ for a head-to-tail dimer. The blueshift of the vC=O band (1756 cm⁻¹) occurs when the C=O group is located close to the S atom from a neighbor molecule (C...S distance 4.0 Å) in a head-to-head dimer. The redshift (1726 cm⁻¹) occurs when the C=O group interacts with the CH₂ groups in the alkoxy chain from a neighbor molecule (O...H distance 2.6 Å) in a head-to-tail dimer. The latter result matches qualitatively the experimental observations. The band related to $\beta_{asym}Ph_{alkoxy}$ and vCS vibrations of the same molecule in a head-to-tail dimer is the weakly blueshifted one at 920 cm⁻¹, which also agrees qualitatively with experimental results. Thus, 11OS5 molecules in a crystal phase are likely in a headto-tail configuration, where C=O groups interact with alkoxy chains. There may be also an intercalated configuration, where C=O groups interact with alkyl chains. The head-to-head configuration is less likely, as it leads to proximity of C=O groups and S atoms from neighbor molecules, which would cause blueshift of the ν C=O band, against the experimental results.

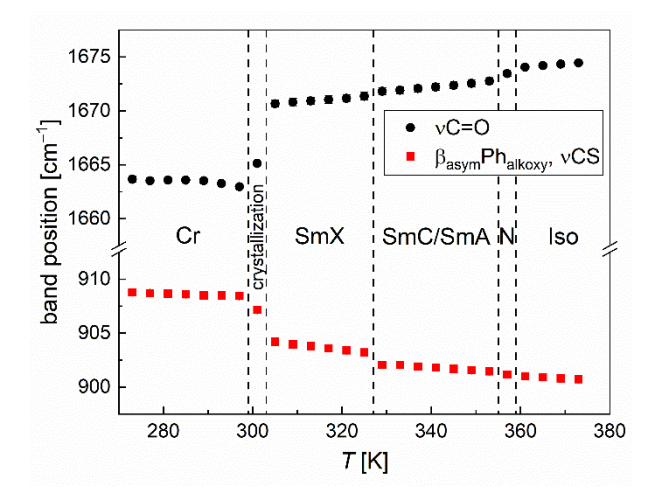


Figure 8. Positions of absorption bands related to ν C=O and $\beta_{asym}Ph_{alkoxy}$, ν CS vibrations in the 11OS5 molecule vs. temperature.

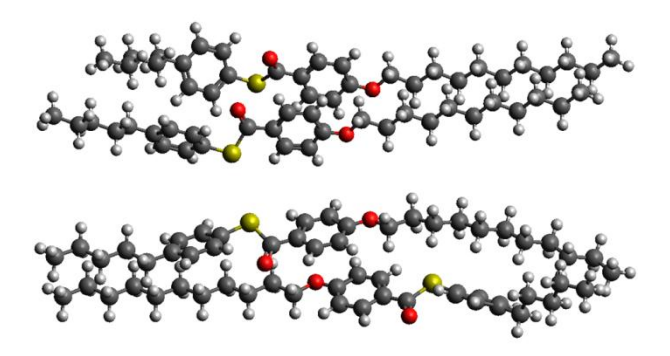


Figure 9. Head-to-head (top) and head-to-tail (bottom) dimers of 11OS5 optimized at the 631+Gd/B3LYP-D3(BJ) level.

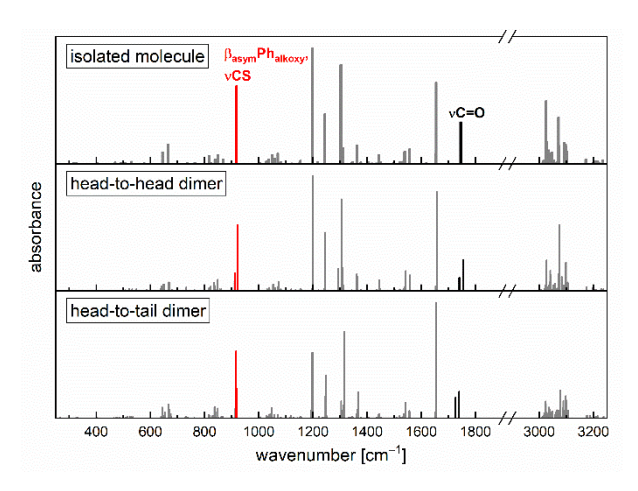


Figure 10. Theoretical unscaled IR spectra calculated for an isolated molecule, head-to-head dimer, and head-to-tail dimer of 11OS5 at the 631+Gd/B3LYP-D3(BJ) level.

4. Summary and conclusions

The isotropic liquid, nematic, smectic A, C, X, and crystal phase of the 11OS5 compound were investigated by dielectric and IR spectroscopies. The dielectric dispersion at 1 kHz is sensitive to all phase transition, including the SmC \rightarrow SmA transition. The dielectric spectra reveal two relaxation processes in the Iso, N, SmA, and SmC phases: low-frequency Maxwell-Wagner-Sillars relaxation and high-frequency molecular s-process, related to rotations around the short molecular axes (flip-flop motion). The MWS process is out of the frequency range in the hexagonal SmX phase. The s-process is also strongly shifted to lower frequencies at the SmC \rightarrow SmX transition, by more of one order of magnitude. The activation energy of the s-process increases to 144 kJ/mol in SmX compared to 94 kJ/mol in SmA and SmC. No relaxation processes are detected in a crystal phase.

The IR absorption bands were assigned to intra-molecular vibrations based on DFT calculations performed with def2TZVPP, def2TZVPP, def2SVPP, def2SVPP, 6311+Gdp, 631+Gd basis sets and B3LYP-D3(BJ) or BLYP-D3(BJ) exchange-correlation functionals. The def2TZVPP/B3LYP-D3(BJ) level of theory provides the lowest root-mean square error between experimental and scaled

calculated band positions (11.6 cm⁻¹). However, def2TZVP/B3LYP-D3(BJ) gives a negligibly higher *RMSE* (11.9 cm⁻¹) with twice as short calculations than for def2TZVPP/B3LYP-D3(BJ). The third best performance is obtained for 631+Gd/B3LYP-D3(BJ), which provides *RMSE* = 12.5 cm⁻¹, while computational time is ten times shorter than for def2TZVPP/B3LYP-D3(BJ). The 631+Gd/B3LYP-D3(BJ) level was further applied for calculations of the theoretical spectra of 11OS5 dimers in head-to-head and head-to-tail configurations.

The IR spectra collected as a function of temperature were analyzed by calculation of the correlation coefficient matrix, which was sensitive to the most of phase transitions except the SmC \rightarrow SmA transition. The k-means cluster analysis performed for the full spectra was sensitive to the N \rightarrow SmA and SmX \rightarrow Cr transition, while the Iso \rightarrow N, SmA \rightarrow SmC transition were not detected and the SmC \rightarrow SmX transition temperature was underestimated. The k-means cluster analysis performed separately in various spectral ranges showed that different intra-molecular vibrations had various sensitivity to particular phase transitions. In some cases, IR spectra collected in the same phase were placed in separate clusters by the algorithm. Thus, the prior knowledge of the phase sequence is necessary and the k-means cluster analysis should be used mainly to indicate which absorption bands are the most sensitive to the phase transition in question, at least in a situation where the ordering of molecules occurs gradually on cooling, as it is for liquid crystals.

The absorption band at 1663-1674 cm⁻¹, related to the C=O stretching, and the band at 901-909 cm⁻¹, related to the in-plane deformations of the aromatic ring close to the alkoxy chain and C-S stretching in the COS group, show the redshift and blueshift with decreasing temperature, respectively. The Iso \rightarrow N and N \rightarrow SmA transitions influence mainly the band at 1663-1674 cm⁻¹ (redshift of ~1 cm⁻¹ at each transition). The IR spectra of SmC and SmA cannot be distinguished by any applied analytical method because the molecular arrangement and, consequently, inter-molecular interactions in these phases are very similar, as the tilt angle in SmC is only 11° and the smectic layer shrinkage between SmA and SmC is ~1% [16]. The redshift/blueshift of the former/latter band at the SmC \rightarrow SmX transition is only ~1 cm⁻¹, despite that the SmX phase is characterized by the long-range positional order in three dimensions. It is caused by the preserved orientational disorder in the SmX phase, detected in dielectric spectra as the s-process. The strongest redshift/blueshift (8/4 cm⁻¹) of the former/latter band occurs during crystallization. It agrees with the absence of dielectric relaxation processes in the solid state, indicating lack of the orientational and conformational disorder in a crystal phase of 11OS5. The DFT calculations for dimers indicate that the C=O group interacts rather with the terminal chains than with the S atom, therefore, the head-to-tail or intercalated configuration in a crystal phase is more likely than the head-to-head configuration.

Acknowledgements. We thank Assoc. Prof. Ewa Juszyńska-Gałązka from Institute of Nuclear Physics Polish Academy of Sciences for discussion regarding data analysis. We gratefully acknowledge Polish high-performance computing infrastructure PLGrid (HPC Center: ACK Cyfronet AGH) for providing computer facilities and support within computational grant no. PLG/2024/017946. Bruker VERTEX 70v FT-IR spectrometer with Advanced Research System DE-202A cryostat and ARS-2HW compressor were purchased thanks to the European Regional Development Fund in the framework of the Innovative Economy Operational Program (contract no. POIG.02.01.00-12-023/08).

Declaration statement: The authors declare no conflict of interest.

Bibliography

- [1] F. Kremer, A. Schönhals (Eds.), Broadband Dielectric Spectroscopy, Springer-Verlag, Berlin Heidelberg 2003, https://doi.org/10.1007/978-3-642-56120-7.
- [2] W. Haase, S. Wróbel (Eds.), Relaxation phenomena. Liquid crystals, magnetic systems, polymers, high-T_c superconductors, metallic glasses, Springer-Verlag, Berlin Heidelberg 2003, https://doi.org/10.1007/978-3-662-09747-2.
- [3] P. Perkowski, M. Urbańska, Dielectric Modes in Antiferroelectric and Ferroelectric Liquid Crystals in a Pure Enantiomeric Version and a Racemic Mixture, Materials 17 (2024) 3335, https://doi.org/10.3390/ma17133335.
- [4] K.Ch. Dey, P.Kr. Mandal, R. Dąbrowski, Effect of lateral fluorination in antiferroelectric and ferroelectric mesophases: synchrotron X-ray diffraction, dielectric spectroscopy and electro-optic study, J. Phys. Chem. Sol. 88 (2016) 14-23, https://doi.org/10.1016/j.jpcs.2015.08.016.
- [5] Ł. Kolek, M. Jasiurkowska-Delaporte, M. Massalska-Arodź, W. Szaj, T. Rozwadowski, Mesomorphic and dynamic properties of 3F5BFBiHex antiferroelectric liquid crystal as reflected by polarized optical microscopy, differential scanning calorimetry and broadband dielectric spectroscopy, J. Mol. Liq. 320 (2020) 114338, https://doi.org/10.1016/j.molliq.2020.114338.
- [6] S. Urban, M. Geppi, Comparison of the dielectric and NMR results for liquid crystals: dynamic aspects, Magn. Reson. Chem. 52 (2014) 656-663, https://doi.org/10.1002/mrc.4100.
- [7] M. Gałązka, E. Juszyńska-Gałązka, A. Bąk, W. Tomczyk, Phase behaviour and dynamics of the liquid crystal 4-ethyl-4'-octylazoxybenzene (4EOB), Phase Trans. 92 (2019) 1089-1101, https://doi.org/10.1080/01411594.2019.1662013.
- [8] T. Rozwadowski, M. Massalska-Arodź, Ł. Kolek, K. Grzybowska, A. Bąk, K. Chłędowska, Kinetics of Cold Crystallization of 4-Cyano-3-fluorophenyl 4-Butylbenzoate (4CFPB) Glass Forming Liquid Crystal. I. Nonisothermal Process As Studied by Microscopic, Calorimetric, and Dielectric Methods, J. Cryst. Growth 15 (2015) 2891-2900, https://doi.org/10.1021/acs.cgd.5b00328.
- [9] D. Georgopoulos, S. Kripotou, E. Argyraki, A. Kyritsis, P. Pissis, Study of Isothermal Crystallization Kinetics of 5CB with Differential Scanning Calorimetry and Broadband Dielectric Spectroscopy, Mol. Cryst. Liq. Cryst. 611 (2015) 197-207, https://doi.org/10.1080/15421406.2015.1030259.
- [10] H.G. Karge, E. Geidel, Vibrational Spectroscopy, in: H.G. Karge, J. Weitkamp, (Eds.), Characterization I. Molecular Sieves Science and Technology, vol 4, Springer-Verlag, Berlin Heidelberg 2004, https://doi.org/10.1007/b94235.
- [11] M. Żurowska, R. Dąbrowski, J. Dziaduszek, K. Garbat, M. Filipowicz, M. Tykarska, W. Rejmer, K. Czupryński, A. Spadło, N. Bennis, J.M. Otón, Influence of alkoxy chain length and fluorosubstitution on mesogenic and spectral properties of high tilted antiferroelectric esters, J. Mater. Chem. 21 (2011) 2144-2153, https://doi.org/10.1039/C0JM02015J.
- [12] K. Milewska, W. Drzewiński, M. Czerwiński, R. Dąbrowski, Design, synthesis and mesomorphic properties of chiral benzoates and fluorobenzoates with direct SmC_A*-Iso phase transition, Liq. Cryst. 42 (2015) 1601-1611, https://doi.org/10.1080/02678292.2015.1078916.
- [13] M. Rogojerov, G. Keresztury, B. Jordanov, Vibrational spectra of partially oriented molecules having two conformers in nematic and isotropic solutions: furfural and 2-chlorobenzaldehyde, Spectrochim. Acta A Mol. Biomol. Spectrosc. 61 (2005) 1661-1670, https://doi.org/10.1016/j.saa.2004.11.043.

- [14] S. Kutsumizu, A. Kawafuchi, Y. Yamamura, T. Udagawa, T. Otaki, M. Masuda, Y. Miwa, K. Saito, Stabilization of Bicontinuous Cubic Phase and Its Two-Sided Nature Produced by Use of Siloxane Tails and Introduction of Molecular Nonsymmetry, Chem. Eur. J. 27 (2021) 10293-10302, https://doi.org/10.1002/chem.202101233.
- [15] E. Juszyńska-Gałązka, W. Zając, Mesomorphic behaviour and vibrational dynamics of nCFPB liquid crystalline homologues, Phase Trans. 92 (2019) 1077-1088, https://doi.org/10.1080/01411594.2019.1669035.
- [16] A. Deptuch, B. Sęk, S. Lalik, M.D. Ossowska-Chruściel, J. Chruściel, M. Marzec, Structural investigation of the liquid crystalline phases of three homologues from the series of 4-pentylphenyl-4'-n-alkyloxythiobenzoates (n = 9, 10, 11), Liq. Cryst. 52 (2025) 157-169, https://doi.org/10.1080/02678292.2024.2417958.
- [17] J.M. Seddon, Structural studies of Liquid Crystals by X-ray Diffraction, in D. Demus, J. Goodby, G.W. Gray, H.-W. Spiess, V. Vill (Eds.), Handbook of Liquid Crystals, WILEY-VCH Verlag GmbH, Weinheim 1998.
- [18] S.M. Ross, Introduction to Probability and Statistics for Engineers and Scientists (Fourth Edition), Elsevier Academic Press 2009, https://doi.org/10.1016/B978-0-12-370483-2.X0001-X.
- [19] Origin Help. 17.7.3.6 Algorithms (K-Means Cluster Analysis), https://www.originlab.com/doc/Origin-Help/KCA-Algorithm, access on 6 May 2025.
- [20] C. Yuan, H. Yang, Research on K-value selection method of K-means clustering algorithm, J 2 (2019) 226-235, https://doi.org/10.3390/j2020016.
- [21] R. Gautam, S. Vanga, F. Ariese, S. Umapathy, Review of multidimensional data processing approaches for Raman and infrared spectroscopy, EPJ Tech. Instrum. 2 (2015) 8, https://doi.org/10.1140/epjti/s40485-015-0018-6.
- [22] M.E. Neubert, R.E. Cline, M.J. Zawaski, P.J. Wildman, A. Ekachai, The Effect on Mesomorphic Properties of Substituting a Sulfur for the Ether Oxygen Atom in the Ester Linkage of 4-Alkylphenyl-4'-Alkyl or Alkoxybenzoates, Mol. Cryst. Liq. Cryst. 76 (1981) 43-77, https://doi.org/10.1080/00268948108074675.
- [23] N. Osiecka-Drewniak, M.A. Czarnecki, Z. Galewski, Investigation of phase transitions in liquid crystal 12BBAA using window clustering of infrared spectra, J. Mol. Liq. 341 (2021) 117233, https://doi.org/10.1016/j.molliq.2021.117233.
- [24] Gaussian 16, Revision C.01, M.J. Frisch, G.W. Trucks, H.B. Schlegel, G.E. Scuseria, M.A. Robb, J.R. Cheeseman, G. Scalmani, V. Barone, G.A. Petersson, H. Nakatsuji, X. Li, M. Caricato, A.V. Marenich, J. Bloino, B.G. Janesko, R. Gomperts, B. Mennucci, H.P. Hratchian, J.V. Ortiz, A.F. Izmaylov, J.L. Sonnenberg, D. Williams-Young, F. Ding, F. Lipparini, F. Egidi, J. Goings, B. Peng, A. Petrone, T. Henderson, D. Ranasinghe, V.G. Zakrzewski, J. Gao, N. Rega, G. Zheng, W. Liang, M. Hada, M. Ehara, K. Toyota, R. Fukuda, J. Hasegawa, M. Ishida, T. Nakajima, Y. Honda, O. Kitao, H. Nakai, T. Vreven, K. Throssell, J.A. Montgomery, Jr., J.E. Peralta, F. Ogliaro, M.J. Bearpark, J.J. Heyd, E.N. Brothers, K.N. Kudin, V.N. Staroverov, T.A. Keith, R. Kobayashi, J. Normand, K. Raghavachari, A.P. Rendell, J.C. Burant, S.S. Iyengar, J. Tomasi, M. Cossi, J.M. Millam, M. Klene, C. Adamo, R. Cammi, J.W. Ochterski, R.L. Martin, K. Morokuma, O. Farkas, J.B. Foresman, D.J. Fox, Gaussian, Inc., Wallingford CT, 2019.
- [25] F. Weigend, R. Ahlrichs, Balanced basis sets of split valence, triple zeta valence and quadruple zeta valence quality for H to Rn: Design and assessment of accuracy, Phys. Chem. Chem. Phys. 7 (2005) 3297-3305, https://doi.org/10.1039/B508541A.
- [26] F. Weigend, Accurate Coulomb-fitting basis sets for H to Rn, Phys. Chem. Chem. Phys. 8 (2006) 1057-1065, https://doi.org/10.1039/B515623H.
- [27] T. Clark, J. Chandrasekhar, G.W. Spitznagel, P.V.R. Schleyer, Efficient diffuse function-augmented basis sets for anion calculations. III. The 3-21+G basis set for first-row elements, Li-F, J. Comput. Chem. 4 (1983) 294-301, https://doi.org/10.1002/jcc.540040303.
- [28] G.W. Spitznagel, T. Clark, P.V.R. Schleyer, W.J. Hehre, An evaluation of the performance of diffuse function-augmented basis sets for second row elements, Na-Cl, J. Comput. Chem. 8 (1987) 1109-1116, https://doi.org/10.1002/jcc.540080807.

- [29] P.M.W. Gill, B.G. Johnson, J.A. Pople, M.J. Frisch, The performance of the Becke-Lee-Yang-Parr (B-LYP) density functional theory with various basis sets, Chem. Phys. Lett. 197 (1992) 499-505, https://doi.org/10.1016/0009-2614(92)85807-M.
- [30] J.-P. Blaudeau, M.P. McGrath, L.A. Curtiss, L. Radom, Extension of Gaussian-2 (G2) theory to molecules containing third-row atoms K and Ca, J. Chem. Phys. 107 (1997) 5016-5021, https://doi.org/10.1063/1.474865.
- [31] C. Lee, W. Yang, R.G. Parr, Development of the Colle-Salvetti correlation-energy formula into a functional of the electron density, Phys. Rev. B, 37 (1988) 785-789, https://doi.org/10.1103/PhysRevB.37.785.
- [32] A.D. Becke, Density-functional thermochemistry. III. The role of exact exchange, J. Chem. Phys. 98 (1993) 5648-5652, https://doi.org/10.1063/1.464913.
- [33] S. Grimme, S. Ehrlich, L. Goerigk, Effect of the damping function in dispersion corrected density functional theory, J. Comput. Chem. 32 (2011) 1456-1465, https://doi.org/10.1002/jcc.21759.
- [34] M.H. Jamróz, Vibrational Energy Distribution Analysis VEDA 4, Warsaw, 2004-2010.
- [35] M.H. Jamróz, Vibrational energy distribution analysis (VEDA): Scopes and limitations, Spectrochim. Acta A 114 (2013) 220-230, https://doi.org/10.1016/j.saa.2013.05.096.
- [36] K.S. Cole, R.H. Cole, Dispersion and Absorption in Dielectrics I. Alternating Current Characteristics, J. Chem. Phys. 9 (1941) 341-351, https://doi.org/10.1063/1.1750906.
- [37] M. Samet, V. Levchenko, G. Boiteux, G. Seytre, A. Kallel, A. Serghe, Electrode polarization vs. Maxwell-Wagner-Sillars interfacial polarization in dielectric spectra of materials: Characteristic frequencies and scaling laws, J. Chem. Phys. 142 (2015) 194703, https://doi.org/10.1063/1.4919877.
- [38] M. Piwowarczyk, E. Juszyńska-Gałązka, M. Gałązka, The Universal Scaling of Dielectric Response as a Tool in the Description of a Complex Dynamic of 4'-Butyl-4-(2-methylbutoxy)azoxybenzene (4ABO5*), Crystals 14 (2024) 95, https://doi.org/10.3390/cryst14010095.
- [39] M. Massalska-Arodź, E. Juszyńska-Gałązka, Partially ordered glass-forming phases relaxation processes and cold crystallization, J. Mol. Liq. 437 (2025) 128572, https://doi.org/10.1016/j.molliq.2025.128572.
- [40] S.L. Srivastava, R. Dhar, Characteristic time of ionic conductance and electrode polarization capacitance in some organic liquids by low frequency dielectric spectroscopy, Indian J. Pure Appl. Phys. 29 (1991) 745-751.
- [41] J. Chruściel, H. Kresse, S. Urban, Megahertz dielectric relaxation process in the nematic and smectic phases of two thiol esters (9S5 and 10S5), Liq.Cryst. 11 (1992) 711-718, https://doi.org/10.1080/02678299208029022.
- [42] J.C. Zapata Trujillo, L.K. McKemmish, Model Chemistry Recommendations for Scaled Harmonic Frequency Calculations: A Benchmark Study, J. Phys. Chem. A 127 (2023) 1715-1735, https://doi.org/10.1021/acs.jpca.2c06908.
- [43] I. Łukaszewska, S. Lalik, A. Bukowczan, M. Marzec, K. Pielichowski, K.N. Raftopoulos, Tailoring the physical properties of non-isocyanate polyurethanes by introducing secondary amino groups along their main chain, J. Mol. Liq. 391 (2023) 123263, https://doi.org/10.1016/j.molliq.2023.123263.
- [44] C. Wang, P. Li, S. Zhang, G. Zhang, S. Tan, Y. Wu, M. Watanabe, Azobenzene Molecular Trigger Controlling Phase Transitions of PNIPAm in Ionic Liquids and Light-Controlled Adhesiveness, Macromolecules 53 (2020) 4901-4907, https://doi.org/10.1021/acs.macromol.0c00652.

Transitions between liquid crystalline phases investigated by dielectric and infra-red spectroscopies

Aleksandra Deptuch^{1,*}, Natalia Osiecka-Drewniak¹, Anna Paliga², Natalia Górska³, Anna Drzewicz¹, Katarzyna Chat¹, Mirosława D. Ossowska-Chruściel⁴, Janusz Chruściel⁴

Supplementary Materials

¹ Institute of Nuclear Physics Polish Academy of Sciences, Radzikowskiego 152, PL-31342 Kraków, Poland

² Faculty of Physics, Astronomy and Applied Computer Science, Jagiellonian University, Łojasiewicza 11, PL-30348 Kraków, Poland

³ Faculty of Chemistry, Jagiellonian University, Gronostajowa 2, PL-30387 Kraków, Poland

⁴ Faculty of Science, University of Siedlee, 3 Maja 54, PL-08110 Siedlee, Poland

^{*} corresponding author, aleksandra.deptuch@ifj.edu.pl

Table S1. The band assignment of the experimental IR spectra of 11OS5 at the room temperature, based on the DFT calculations (**def2TZVPP** basis set, **B3LYP-D3(BJ)** functional). Notations: β – in-plane deformation, γ – out-of-plane deformation, δ – scissoring, ν – stretching, ρ – rocking, τ – twisting, ω – wagging.

experimental peak position [cm ⁻¹]	unscaled calculated peak position [cm ⁻¹]	scaled calculated peak position [cm ⁻¹]	vibration (contribution $\geq 10\%$)
384	387	377	58% δCCC _{alkyl}
401	403	393	27% δCCC _{alkoxy}
416	417	406	83% yPh _{alkyl}
445	448	436	20% δCCO _{alkoxy}
468	472	460	40% δCCC _{alkoxy}
484	495	482	12% γPh _{alkyl}
500	505	492	40% SCCC _{alkyl}
506	515	502	73% γPh _{alkoxy}
523	532	518	49% δCOC _{alkoxy}
570	579	564	30% β _{asym} Ph _{alkoxy} , 10% δCOC _{alkoxy} , 10% δCSC/Ph _{alkyl}
628	648	631	65% β _{asym} Ph _{alkoxy}
641	657	640	51% γCOS, 16% γPh _{alkoxy}
661	669	652	$44\% \beta_{\text{asym}} \text{Ph}_{\text{alkoxy}}$
670	680	662	58% β_{sym} Phalkyl
			1 .
723 733	734 742	715 723	83% ρCH _{2alkoxy}
733 750	742 766	723 746	71% ρCH _{2alkyl}
750	766	746	22% ρCH _{2alkyl} , 17% γPh _{alkyl}
781	792	772	45% pCH _{2alkoxy}
803	822	801	51% γPh _{alkyl}
819	841	819	$47\% \beta_{asym} Ph_{alkoxy}$
839	863	841	76% γPh _{alkoxy}
851	871	848	49% γPh _{alkyl} , 20% τCH _{2alkyl}
906	919	895	29% β_{asym} Ph _{alkoxy} , 26% vCS
934	993	967	74% νCC _{alkoxy}
946	1001	975	57% νCC _{alkoxy}
987	1028	1001	69% νCC _{alkoxy}
1015	1048	1021	41% νCO _{alkoxy}
1023	1066	1038	59% νCC _{alkoxy}
1051	1076	1048	67% νCC _{alkoxy}
1095	1120	1091	75% $\beta_{asym}Ph_{alkyl}$
1119	1150	1120	54% v _{sym} CCC _{alkoxy}
1168	1189	1158	73% $\beta_{sym}Ph_{alkoxy}$
1212	1238	1206	69% β _{asym} Ph _{alkoxy}
1231	1266	1233	59% ωCH _{2alkyl}
1269	1296	1262	66% β _{asym} Ph _{alkoxy}
1310	1348	1313	69% β _{asym} Ph _{alkoxy}
1323	1355	1320	40% ωCH _{2alkyl} , 25% β _{asym} Ph _{alkyl}
1353	1370	1335	61% ωCH _{2alkoxy}
1378	1395	1359	55% ωCH _{2alkyl}
1400	1432	1395	65% ωCH _{2alkoxy}
1421	1444	1407	53% β _{asym} Ph _{alkyl}
1435	1477	1439	81% δCH _{2alkyl}
1468	1523	1484	81% δCH2alkyl 81% δCH2alkoxy
1495	1535	1495	67% $\beta_{\text{asym}} Ph_{\text{alkyl}}$
1508	1549	1509	63% β _{asym} Ph _{alkoxy}
1600	1646	1603	70% β _{sym} Ph _{alkoxy}
1661	1736	1691	89% vC=O
2849	3017	2871	74% v _{sym} CH _{2alkoxy}
2872	3034	2887	93% v _{sym} CH _{2alkoxy}
2915	3060	2912	83% $v_{asym}CH_{2alkoxy}$
2956	3078	2929	75% vasymCH2alkoxy
3041	3190	3035	97% ν _{asym} CH/Ph _{alkoxy}
3049	3200	3045	88% ν_{sym} CH/Ph _{alkyl}
3060	3221	3065	99% v _{sym} CH/Ph _{alkoxy}

Table S2. The band assignment of the experimental IR spectra of 11OS5 at the room temperature, based on the DFT calculations (**def2TZVP** basis set, **B3LYP-D3(BJ)** functional). Notations: β – in-plane deformation, γ – out-of-plane deformation, δ – scissoring, ν – stretching, ρ – rocking, τ – twisting, ω – wagging.

experimental peak position [cm ⁻¹]	unscaled calculated peak position [cm ⁻¹]	scaled calculated peak position [cm ⁻¹]	vibration (contribution $\geq 10\%$)
384	388	378	59% δCCC _{alkyl}
401	403	393	25% δ CCC _{alkoxy}
416	415	404	80% γPh _{alkyl}
445	448	437	30% δ CCC _{alkoxy}
468	472	460	46% δCCO _{alkoxy}
484	495	482	13% γPhalkyl, 11% δCCOalkoxy
500	505	492	44% δCCC _{alkyl}
506	514	502	•
523			67% γPh _{alkoxy}
	532	519	45% δCOC _{alkoxy}
570	579	564	25% β _{asym} Ph _{alkoxy} , 12% δCOC _{alkoxy}
628	647	631	$66\% \beta_{asym} Ph_{alkoxy}$
641	657	640	77% γPh _{alkoxy}
661	669	652	51% β_{asym} Ph _{alkoxy}
670	680	663	45% $\beta_{sym}Ph_{alkyl}$
723	735	715	68% ρCH _{2alkoxy}
733	742	723	67% ρCH _{2alkyl}
750	766	747	36% ρCH _{2alkyl}
781	792	772	46% ρCH _{2alkoxy}
803	820	799	56% γPh _{alkyl}
819	841	820	60% β _{asym} Ph _{alkoxy}
839	860	838	82% γPh _{alkoxy}
851	869	847	48% γPh _{alkyl} , 10% ρCH _{2alkyl}
906	919	896	29% β _{asym} Ph _{alkoxy} , 25% νCS
934	993	968	66% vCC _{alkoxy}
946	1001	976	69% vCC _{alkoxy}
987	1028	1002	57% vCC _{alkoxy}
1015	1048	1021	51% vCCalkoxy
1023	1048	1040	73% vCCalkoxy
1051	1077	1050	66% vCCalkoxy
1095	1120	1091	69% β _{asym} Ph _{alkyl}
1119	1150	1121	35% v _{sym} CCC _{alkoxy} , 12% ωCH _{2alkoxy}
1168	1188	1158	61% β _{sym} Ph _{alkoxy}
1212	1238	1206	$70\% \beta_{asym} Ph_{alkoxy}$
1231	1265	1233	56% ωCH _{2alkyl}
1269	1295	1262	49% νCO _{alkoxy} , 11% β _{asym} Ph _{alkoxy}
1310	1348	1314	61% $\beta_{asym}Ph_{alkoxy}$
1323	1354	1319	48% ωCH _{2alkyl} , 25% β _{asym} Ph _{alkyl}
1353	1369	1334	58% ωCH _{2alkoxy}
1378	1395	1359	53% ωCH _{2alkyl}
1400	1430	1393	70% ωCH _{2alkoxy}
1421	1443	1406	57% β _{asym} Ph _{alkyl} , 11% ωCH _{2alkyl}
1435	1476	1438	69% δCH _{2alkyl}
1468	1522	1483	69% δCH _{2alkoxy}
1495	1534	1495	58% β _{asym} Ph _{alkyl}
1508	1548	1508	50% β _{asym} Ph _{alkoxy} , 12% νCO _{alkoxy}
1600	1646	1604	66% β _{sym} Ph _{alkoxy}
1661	1736	1692	89% νC=O
2849	3017	2871	85% v _{sym} CH _{2alkoxy}
2872	3034	2887	92% v _{sym} CH _{2alkoxy}
2915	3060	2912	90% vasymCH2alkoxy
2956	3077	2928	90% $v_{asym}CH_{2alkoxy}$
3041	3190	3036	98% vasymCH/Phalkoxy
3049	3199	3044	88% $v_{sym}CH/Ph_{alkyl}$
3060	3220	3064	85% v _{sym} CH/Ph _{alkoxy} , 15% v _{sym} CH _{2alkoxy}

Table S3. The band assignment of the experimental IR spectra of 11OS5 at the room temperature, based on the DFT calculations (**def2SVPP** basis set, **B3LYP-D3(BJ)** functional). Notations: β – in-plane deformation, γ – out-of-plane deformation, δ – scissoring, ν – stretching, ρ – rocking, τ – twisting, ω – wagging.

experimental peak position [cm ⁻¹]	unscaled calculated peak position [cm ⁻¹]	scaled calculated peak position [cm ⁻¹]	vibration (contribution $\geq 10\%$)
384	389	376	65% δCCC _{alkyl}
401	406	392	16% δCCC _{alkoxy}
416	421	407	70% γPh _{alkyl}
445	452	436	17% δCCO _{alkoxy}
468	476	460	54% δCCC _{alkoxy} , 10% νCS
484	500	483	11% δCCC _{alkyl}
500	507	490	41% δCCC _{alkyl}
506	521	503	72% γPh _{alkoxy}
523	535	517	41% δ CCC _{alkoxy}
			*
570	582	562	16% β _{asym} Ph _{alkoxy} , 11% δCSC/Ph _{alkyl}
628	647	625	77% $\beta_{\text{asym}} Ph_{\text{alkoxy}}$
641	656	633	83% γPh _{alkoxy}
661	671	648	26% β _{asym} Ph _{alkoxy}
670	680	657	29% β _{sym} Ph _{alkyl} , 21% vSC/Ph _{alkyl}
723	744	718	77% ρCH _{2alkoxy}
733	751	725	76% ρCH _{2alkyl}
750	772	745	15% γPh _{alkyl} , 11% ρCH _{2alkyl}
781	798	771	49% ρCH _{2alkoxy}
803	824	796	44% γPh _{alkyl} , 10% ρCH _{2alkyl}
819	846	817	56% β _{asym} Ph _{alkoxy}
839	868	838	75% γPh _{alkoxy}
851	873	843	34% γPh _{alkyl} , 17% ρCH _{2alkyl}
906	928	896	37% vCS, 23% β _{asym} Ph _{alkoxy}
934	1014	979	68% vCC _{alkoxy}
946	1026	991	74% β _{asym} Ph _{alkoxy}
987	1035	999	65% β _{asym} Ph _{alkyl}
1015	1084	1041	68% vCC _{alkoxy}
1023	1090	1047	69% vCCalkoxy
1051	1118	1073	•
			40% v _{sym} CCC _{alkoxy}
1095	1136	1091	89% β _{sym} Ph _{alkoxy}
1119	1154	1108	47% v _{sym} CCC _{alkoxy}
1168	1181	1134	87% β _{sym} Ph _{alkoxy}
1212	1248	1198	59% $\beta_{asym}Ph_{alkoxy}$
1231	1301	1249	60% ωCH _{2alkoxy}
1269	1325	1272	59% β _{asym} Ph _{alkoxy}
1310	1377	1322	52% β _{asym} Ph _{alkoxy}
1323	1399	1343	58% ωCH _{2alkoxy}
1353	1401	1345	60% ωCH _{2alkyl}
1378	1419	1362	50% ωCH _{2alkoxy}
1400	1446	1388	46% ωCH _{2alkoxy}
1421	1449	1391	52% β _{asym} Ph _{alkyl} , 11% ωCH _{2alkyl}
1435	1482	1423	98% δCH_{3alkyl}
1468	1512	1452	74% δCH _{2alkoxy}
1495	1538	1477	76% β _{asym} Ph _{alkyl}
1508	1558	1496	81% β _{asym} Ph _{alkoxy}
1600	1671	1604	72% β _{sym} Ph _{alkoxy}
1661	1787	1716	91% vC=O
2849	3006	2862	82% v _{sym} CH _{2alkoxy}
2872	3025	2880	96% v _{sym} CH _{2alkoxy}
2915	3060	2914	89% vasymCH2alkoxy
2956	3079	2932	80% $v_{asym}CH_{2alkoxy}$
3041	3191	3039	95% vasymCH/Phalkoxy
3049	3203	3050	95% v_{sym} CH/Ph _{alkyl}
3060	3219	3065	90% v _{sym} CH/Ph _{alkoxy}

Table S4. The band assignment of the experimental IR spectra of 11OS5 at the room temperature, based on the DFT calculations (**def2SVP** basis set, **B3LYP-D3(BJ**) functional). Notations: β – in-plane deformation, γ – out-of-plane deformation, δ – scissoring, ν – stretching, ρ – rocking, τ – twisting, ω – wagging.

experimental peak position [cm ⁻¹]	unscaled calculated peak position [cm ⁻¹]	scaled calculated peak position [cm ⁻¹]	vibration (contribution $\geq 10\%$)
384	388	376	57% δCCC _{alkyl}
401	406	393	44% δCCC _{alkoxy}
416	421	408	67% γPh _{alkyl}
445	451	437	20% δCCC _{alkoxy}
468	475	460	47% δCCC _{alkoxy}
484	499	483	21% γPh _{alkyl}
500	507	491	32% δCCC _{alkyl} , 18% γPh _{alkyl}
506	520	504	74% γ Ph _{alkoxy}
523	535	518	45% δCCO _{alkoxy} , 11% γPh _{alkyl}
570	581	563	11% β _{asym} Ph _{alkoxy} , 10% δCCO _{alkoxy}
628	646	626	47% β _{asym} Ph _{alkoxy}
641	655	634	60% γCOS, 14% γPh _{alkoxy}
661	671	650	37% β _{asym} Ph _{alkoxy}
670	680	659	60% β _{sym} Ph _{alkyl}
723	741	718	69% ρCH _{2alkoxy}
733	745 767	722 743	69% pCH _{2alkyl}
750	767	743	18% ρCH _{2alkyl} , 15% γPh _{alkyl}
781	790	765 704	61% ρCH _{2alkoxy}
803	820	794	51% ρCH _{2alkyl}
819	846	819	$57\% \beta_{asym} Ph_{alkoxy}$
839	866	839	62% γPh _{alkoxy}
851	867	840	35% γPh _{alkyl} , 11% γPh _{alkoxy}
906	928	899	40% vCS, 25% β _{asym} Ph _{alkoxy}
934	1012	980	75% νCC _{alkoxy}
946	1022	990	73% $\beta_{asym}Ph_{alkoxy}$
987	1032	1000	74% $\beta_{asym}Ph_{alkoxy}$
1015	1081	1043	55% νCC _{alkoxy}
1023	1088	1049	57% νCC _{alkoxy}
1051	1113	1073	36% νCC _{alkoxy}
1095	1132	1092	89% $\beta_{asym}Ph_{alkoxy}$
1119	1150	1109	72% v _{sym} CCC _{alkoxy}
1168	1177	1135	88% β _{sym} Ph _{alkoxy}
1212	1246	1202	66% β _{asym} Ph _{alkoxy}
1231	1287	1241	60% ωCH _{2alkoxy}
	1320	1273	26% ωCH _{2alkoxy} , 21% β _{asym} Ph _{alkoxy}
1269	1326	1279	27% ωCH _{2alkoxy} , 20% β _{asym} Ph _{alkoxy}
1310	1374	1325	58% β _{asym} Ph _{alkoxy}
1323	1386	1337	61% ωCH _{2alkoxy}
1353	1389	1341	50% ωCH _{2alkyl}
1378	1407	1357	66% ω CH _{2alkoxy} , 10% ν CC _{alkoxy}
1400	1435	1384	51% ωCH _{2alkoxy}
1421	1443	1392	52% β _{asym} Ph _{alkyl} , 15% ωCH _{2alkyl}
1435	1471	1419	98% 8CH3alkyl
	1500	1447	60% δCH _{2alkoxy}
1468			
1495	1530	1476	$80\% \beta_{asym} Ph_{alkyl}$
1508	1552	1497	80% β _{asym} Ph _{alkoxy}
1600	1667	1608	75% β _{sym} Ph _{alkoxy}
1661	1787	1724	90% vC=O
2849	3018	2866	87% v _{sym} CH _{2alkoxy}
2872	3038	2885	96% v _{sym} CH _{2alkoxy}
2915	3071	2916	91% $v_{asym}CH_{2alkoxy}$
2956	3090	2934	84% v _{asym} CH _{2alkoxy}
3041	3196	3035	95% ν_{asym} CH/Ph _{alkoxy}
3049	3207	3045	97% v _{sym} CH/Ph _{alkyl}
3060	3224	3061	99% v _{sym} CH/Ph _{alkoxy}

Table S5. The band assignment of the experimental IR spectra of 11OS5 at the room temperature, based on the DFT calculations (**def2SVP** basis set, **BLYP-D3(BJ**) functional). Notations: β – in-plane deformation, γ – out-of-plane deformation, δ – scissoring, ν – stretching, ρ – rocking, τ – twisting, ω – wagging.

experimental peak position [cm ⁻¹]	unscaled calculated peak position [cm ⁻¹]	scaled calculated peak position [cm ⁻¹]	vibration (contribution $\geq 10\%$)
384	378	380	61% δCCC _{alkyl}
401	392	394	34% δCCC _{alkoxy} , 10% vCS
416	423	425	33% v _{asym} CSC/Ph _{alkyl} , 10% δCCC _{alkyl}
445	438	440	12% δCCO _{alkoxy}
468	460	462	47% δCOC/Ph _{alkoxy}
484	485	487	11% δCOC _{alkoxy}
500	493	495	40% δCCC _{alkyl}
506	504	506	30% SCCC _{alkoxy}
523	519	522	49% δCOC _{alkoxy}
570	560	563	23% δCSC/Phalkyl, 20% δCCC _{alkyl} , 12% δCOC _{alkoxy}
628	627	630	58% β _{asym} Ph _{alkoxy} , 11% γCOS
641	629	632	52% γCOS, 12% γPhalkoxy
661	647	650	
			$42\% \beta_{\text{asym}} \text{Ph}_{\text{alkoxy}}$
670	657	660	31% vSC/Ph _{alkyl} , 18% β _{sym} Ph _{alkyl}
723	730	734	75% pCH _{2alkyl}
733	737	741 750	74% γPh _{alkoxy}
750	746	750	36% ρCH _{2alkyl} , 27% γPh _{alkyl}
781	772	776	37% ρCH _{2alkoxy}
803	796	800	58% ρCH _{2alkyl}
819	814	818	$34\% \beta_{asym} Ph_{alkoxy}$
839	837	841	$78\% \gamma Ph_{alkoxy}$
851	842	846	40% ρCH _{2alkyl} , 11% γPh _{alkyl}
906	888	892	36% vCS, 33% β _{asym} Ph _{alkoxy}
934	956	961	$88\% \ \gamma Ph_{alkoxy}$
946	962	967	92% γPh _{alkyl}
987	974	979	50% νCC _{alkoxy}
1015	1002	1005	49% νCC _{alkoxy}
1023	1013	1016	40% νCO _{alkoxy}
1051	1047	1051	51% νCC _{alkoxy}
1095	1078	1082	75% β _{asym} Ph _{alkyl}
1119	1102	1106	88% β_{sym} Ph _{alkoxy}
1168	1144	1148	73% β_{sym} Ph _{alkoxy}
1212	1202	1206	66% β _{asym} Ph _{alkoxy}
1231	1219	1223	53% ωCH _{2alkyl}
1269	1265	1269	55% νCO _{alkoxy} , 14% β _{asym} Ph _{alkoxy}
1310	1340	1345	65% β _{sym} Ph _{alkoxy}
1323	1345	1350	33% ωCH _{2alkoxy} , 13% β _{sym} Ph _{alkoxy}
1353	1350	1355	57% ωCH _{2alkyl} , 14% β _{sym} Ph _{alkyl}
1378	1359	1364	67% ωCH _{2alkoxy}
1400	1384	1389	52% ωCH _{2alkoxy}
1421	1396	1401	60% β _{asym} Ph _{alkyl} , 13% ωCH _{2alkyl}
1435	1432	1437	86% δ CH _{3alkyl}
1468	1457	1462	69% δ CH _{2alkoxy}
1495	1478	1483	77% $\beta_{\text{asym}} Ph_{\text{alkyl}}$
1508	1494	1499	57% β _{asym} Ph _{alkoxy}
1600	1603	1608	67% β _{sym} Ph _{alkoxy}
1661	1707	1713	90% νC=O
2849	2939	2866	79% v _{sym} CH _{2alkoxy}
2872	2958	2885	96% v _{sym} CH _{2alkoxy}
2915	2988	2914	91% vasymCH2alkoxy
2956	3006	2932	83% v _{asym} CH _{2alkoxy}
3041	3113	3036	96% vasymCH/Phalkoxy
3049	3124	3047	99% v _{sym} CH/Ph _{alkyl}
3060	3141	3063	100% v _{sym} CH/Ph _{alkoxy}

Table S6. The band assignment of the experimental IR spectra of 11OS5 at the room temperature, based on the DFT calculations (6311+Gdp basis set, B3LYP-D3(BJ) functional). Notations: β – in-plane deformation, γ – out-of-plane deformation, δ – scissoring, ν – stretching, ρ – rocking, τ – twisting, ω – wagging.

experimental peak position [cm ⁻¹]	unscaled calculated peak position [cm ⁻¹]	scaled calculated peak position [cm ⁻¹]	vibration (contribution $\geq 10\%$)
384	381	373	35% δCCC _{alkoxy} , 13% δOCC/Ph _{alkoxy}
401	402	393	25% SCCC _{alkoxy}
416	422	413	28 % vSC, 25% δCCC _{alkyl}
445	447	437	17% δCCC _{alkoxy}
468	473	463	13% δOCC/Ph _{alkoxy}
484	507	496	32% δ CCC _{alkoxy}
500	508	497	77% γPh _{alkoxy}
506	519	508	38% δCCC _{alkoxy}
523	546	534	17% γPhalkyl
570	585	572	14% γPh _{alkyl}
628	645	631	74% β _{asym} Ph _{alkoxy}
641	646	632	
			80% γPh _{alkoxy}
661	665	650	$40\% \beta_{\rm asym} Ph_{\rm alkoxy}$
670	673	658	30% β _{sym} Ph _{alkyl}
723	733	717	65% ρCH _{2alkyl}
733	742	726	73% pCH _{2alkoxy}
750	757	740	75% γPh _{alkyl}
781	791	774	53% ρCH _{2alkoxy}
803	824	806	$49\% \ \gamma Ph_{alkyl}$
819	838	820	29% νCC _{alkoxy} , 17% νCO _{alkoxy} ,
019	636	820	13% $\beta_{asym}Ph_{alkoxy}$
839	850	831	68% γPh _{alkoxy}
851	850	831	49% γPh _{alkyl}
906	914	894	24% vCS, 22% β _{asym} Ph _{alkoxy}
934	985	963	86% γPh _{alkoxy}
946	999	977	55% vCC _{alkoxy}
987	1025	1002	41% νCC _{alkoxy} , 21% β _{asym} Ph _{alkoxy}
1015	1044	1018	49% vCO _{alkoxy}
1023	1064	1037	70% vCCalkoxy
1051	1075	1048	63% vCC _{alkoxy}
1095	1114	1086	78% β _{asym} Ph _{alkyl}
1119	1147	1118	
1168	1186	1156	58% v _{sym} CCC _{alkoxy}
			62% β _{sym} Ph _{alkoxy}
1212	1236	1205	71% β _{asym} Ph _{alkoxy}
1231	1266	1234	67% ωCH _{2alkoxy}
1269	1290	1258	46% νCO _{alkoxy} , 23% β _{asym} Ph _{alkoxy}
1310	1347	1313	$72\% \beta_{asym} Ph_{alkoxy}$
1323	1348	1314	52% β _{asym} Ph _{alkyl} , 14% τCH _{2alkyl}
1353	1365	1331	65% ωCH _{2alkoxy}
1378	1413	1377	83% δCH _{3alkoxy}
1400	1430	1394	57% ωCH _{2alkoxy}
1421	1435	1399	37% τCH _{2alkyl} , 34% β _{asym} Ph _{alkyl}
1435	1500	1462	99% δCH _{3alkyl}
1468	1521	1483	68% δCH _{2alkoxy}
1495	1525	1487	73% β _{asym} Ph _{alkyl}
1508	1542	1503	47% β _{asym} Ph _{alkoxy}
1600	1643	1602	71% β _{sym} Ph _{alkoxy}
1661	1742	1698	90% vC=O
2849	3012	2870	86% v _{sym} CH _{2alkoxy}
	3032		
2872		2889	94% v _{sym} CH _{2alkoxy}
2915	3057	2913	$82\% v_{asym}CH_{2alkoxy}$
2956	3079	2934	84% v _{asym} CH _{2alkyl}
3041	3186	3036	96% v _{asym} CH/Ph _{alkoxy}
3049	3190	3040	94% vasymCH/Phalkyl
3060	3214	3062	100% ν _{sym} CH/Ph _{alkoxy}

Table S7. The band assignment of the experimental IR spectra of 11OS5 at the room temperature, based on the DFT calculations (631+Gd basis set, B3LYP-D3(BJ) functional). Notations: β – in-plane deformation, γ – out-of-plane deformation, δ – scissoring, ν – stretching, ρ – rocking, τ – twisting, ω – wagging.

experimental	unscaled calculated	scaled calculated	vibration (contribution $\geq 10\%$)
peak position [cm ⁻¹]	peak position [cm ⁻¹]	peak position [cm ⁻¹]	
384	387	378	55% δCCC _{alkyl}
401	404	395	14% δCCC _{alkoxy}
416	433	423	35% vCS
445	448	438	31% δCCC _{alkoxy}
468	470	459	26% &CCC _{alkoxy}
484	492	481	27% γPh_{alkyl}
500	503	491	43% &CCC _{alkyl}
506	508	496	84% γPh _{alkoxy}
523	531	519	43% δCCO _{alkoxy}
570	577	564	21% δCCC _{alkoxy} , 13% β _{asym} Ph _{alkoxy} , 10% νCS
628	645	630	52% β _{asym} Ph _{alkoxy} , 14% δCCC _{alkoxy}
641	646	631	75% γCOS, 13% γPh _{alkoxy}
661	666	650	$39\% \beta_{asym} Ph_{alkoxy}$
670	677	661	29% vSC/Ph _{alkyl} , 20% β _{sym} Ph _{alkyl}
723	736	719	73% ρCH _{2alkoxy}
733	743	726	74% ρCH _{2alkyl}
750	765	747	32% ρCH _{2alkyl} , 23% γPh _{alkyl}
781	795	776	51% ρCH _{2alkoxy}
803	818	799	$67\% \ \gamma Ph_{alkyl}$
819	839	819	29% β _{asym} Ph _{alkoxy} , 18% νCO _{alkoxy}
839	850	830	$46\% \ \gamma Ph_{alkoxy}$
851	870	850	36% γPh _{alkyl} , 21% ρCH _{2alkyl}
906	919	898	35% vCS, 26% β _{asym} Ph _{alkoxy}
934	982	959	80% γPh _{alkoxy}
946	1004	981	64% νCC _{alkoxy}
987	1029	1005	62% β _{asym} Ph _{alkoxy} , 18% νCC _{alkoxy}
1015	1051	1015	45% νCC _{alkoxy}
1023	1071	1035	68% νCC _{alkoxy}
1051	1081	1044	73% νCC _{alkoxy}
1095	1122	1084	70% νSC/Ph _{alkoxy}
1119	1154	1115	68% $\beta_{sym}Ph_{alkoxy}$
1168	1198	1157	90% β _{sym} Ph _{alkoxy}
1212	1245	1203	71% $\beta_{asym}Ph_{alkoxy}$
1231	1271	1228	53% ωCH _{2alkoxy}
1269	1303	1259	52% v _{asym} COC _{alkoxy} , 12% β _{asym} Ph _{alkoxy}
1310	1363	1317	36% β _{sym} Ph _{alkoxy} , 14% ωCH _{2alkyl}
1323	1364	1318	24% ωCH _{2alkyl} , 20% β _{asym} Ph _{alkyl}
1353	1377	1330	51% ωCH _{2alkoxy}
1378	1434	1385	83% ωCH _{3alkyl}
1400	1443	1394	57% ωCH _{2alkoxy}
1421	1450	1401	52% β _{asym} Ph _{alkyl} , 14% ωCH _{2alkyl}
1435	1522	1470	82% δCH _{3alkyl} , 10% τCH _{2alkoxy}
1468	1539	1487	67% δCH _{2alkoxy}
1495	1541	1489	63% β _{asym} Ph _{alkyl}
1508	1557	1504	42% $\beta_{asym}Ph_{alkoxy}$
1600	1655	1599	73% β _{sym} Ph _{alkoxy}
1661	1746	1687	89% vC=O
2849	3025	2866	81% v _{sym} CH _{2alkoxy}
2872	3046	2886	95% v _{sym} CH _{2alkoxy}
2915	3071	2910	82% vasymCH2alkoxy
2956	3093	2930	90% v _{asym} CH _{2alkoxy}
3041	3209	3040	93% vasymCH/Phalkyl
3049	3216	3047	94% v _{asym} CH/Ph _{alkyl}
		,	asym Cara ankyr

Table S8. The band assignment of the experimental IR spectra of 11OS5 at the room temperature, based on the DFT calculations (631+Gd basis set, BLYP-D3(BJ) functional). Notations: β – in-plane deformation, γ – out-of-plane deformation, δ – scissoring, ν – stretching, ρ – rocking, τ – twisting, ω – wagging.

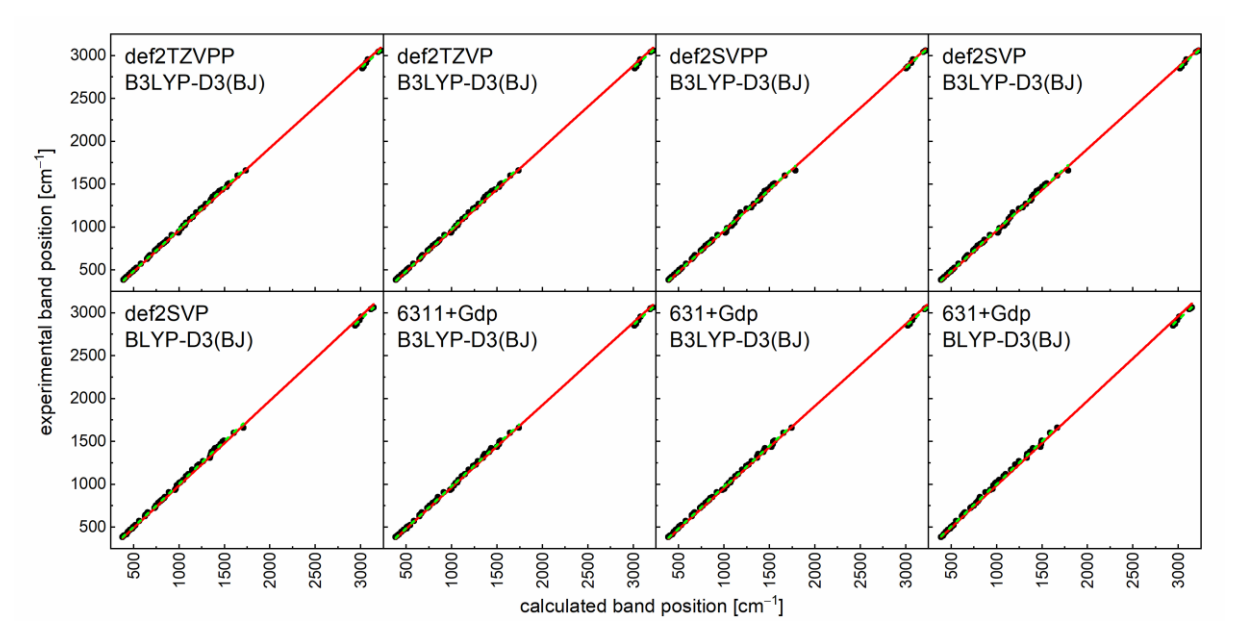


Figure S1. Experimental band positions in the IR spectrum of 11OS5 in the crystal phase in the room temperature vs. calculated band positions at different levels of theory. Solid and dashed lines indicate linear fits with intercept fixed to zero in the full spectral range and separate in the $<1000 \text{ cm}^{-1}$, $1000-2000 \text{ cm}^{-1}$, $>2000 \text{ cm}^{-1}$ ranges, respectively.

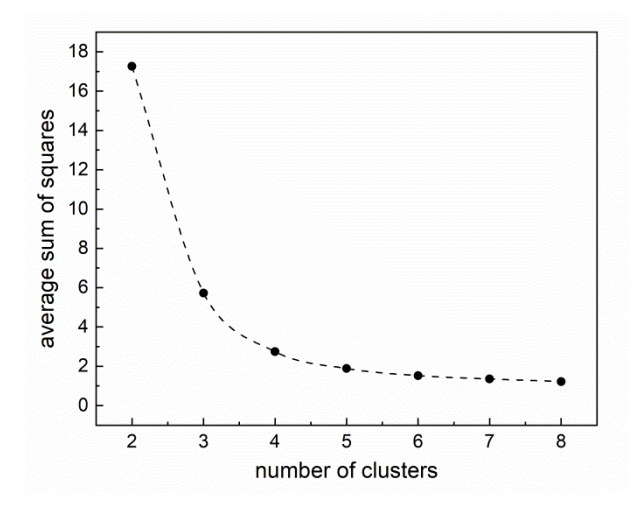


Figure S2. Determination of an optimal number of clusters in the k-means cluster analysis by the "elbow method".